Near Surface Geophysics, 2016, **14**, pp. 39 - 45 doi:10.3997/1873-0604.2015047

On the geoelectric structure of the Sphinx Area in Egypt

Pavel O. Barsukov and Eduard B. Fainberg*

Institute of Physics of the Earth RAS, Russia

Received June 2014, revision accepted June 2015

ABSTRACT

A three-dimensional model of the electrical resistivity of rocks to a depth of 150 m in the Sphinx and the Pyramid of Khephren (Giza, Egypt) area was built using the results of transient electromagnetic soundings. The technology of the soundings, the data processing, and the design of the media's model as a result of three-dimensional block inversion are described. The boundary of the Paleogene limestones that form the plateau of the pyramids and the underlying structure of the folded Cretaceous are defined based on geological interpretation.

The created plateau model indicated the thickness of the slightly inclined Mokattam limestones varied from 25 m to 150 m within a 1000 × 300 m^2 area. Such intense changes in the limestone subface's altitudes were controlled by the folded structure of the underlying Cretaceous carbonates. Cretaceous carbonates show low electrical resistivity, which is typical for fractured rocks saturated with saline water. Dense Mokattam limestone blocks are broken by water-saturated zones with subvertical faults in the southwest–northeast direction. The electrical resistivity in the carbonate surface layer, which lies at the base of the pyramids and Sphinx, is heterogeneous with a composition that depends on the clay content and presence of halite.

INTRODUCTION

In April 1994, a joint project between National Research Institute of Astronomy and Geophysics (NRIAG, Egypt) and Russian Academy of Sciences (RAS) (Barsukov *et al.* 1996) using a transient electromagnetic method (TEM) was conducted on the Sphinx and Pyramid of Khephren (p. Khephren) area (Fig. 1). The purpose of the research was to evaluate the configuration of aquifers and groundwater reservoirs, and combine the data with the results of the prior NRIAG vertical electrical soundings (VES) in the vicinity of the Sphinx monument.

A square single-turn wire coincident antenna of 50×50 m and TEM-FAST technology (Barsukov, Fainberg, and Khabensky 2007) of soundings were used to excite and measure the electromagnetic (EM) fields. The transient responses of the medium on the pulse excitation fields were measured in the time range of 4 μs–1000 μs, with output transmitter current of 1 A, the voltage range of 1 μV–12 V, provided that the information on the electrical resistivity of rocks is at depths of 2–5 m–150 m. One of the factors that complicate the measurement of TEM responses is the presence of power lines and metal objects in the study area, which significantly distort the measurement data and create intense noise. Therefore, the additional control measurements were performed away from the pyramids in the uncontaminated-by-noise western plateau within the Mokattam formation. TEM soundings were carried out in 46 points (Fig. 2). In this paper, we use these data to study the geoelectric structure and geologic section of the Mokattam formation.

The technology of TEM-FAST soundings

The applied technology of the soundings is based on the analysis of transient responses of the medium to the pulsed EM excitation.

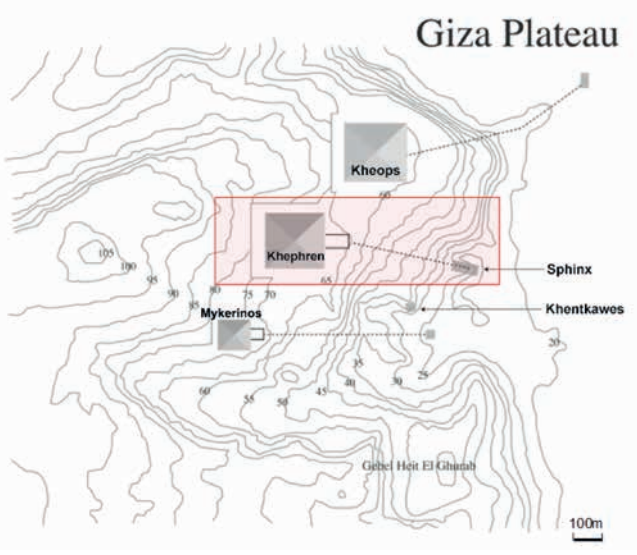

Figure 1 The area under investigation; the red rectangle shows the area (1000×300 m^2) of TEM soundings and 3D inversion. The contours show the topography of the Earth's surface (MSL). The dotted line shows the underground entrances to the pyramids.

* fain@igemi.troitsk.ru

A square wire antenna with a side length of 5 m to 500 m is placed on the ground. The transmitter excites the pulses of electric current with a steep end-off, and the receiver registers in the same antenna (coincident loop configuration) step-off transient responses during the pauses between the pulses. The depth h_t of the sounding (diffusion depth) is controlled by the time t measured from the end-off of the pulses. For a uniform medium of resistivity ρ and magnetic permeability μ, the depth h_t is defined as (e.g., Zhdanov 2009; Kamenetsky, Stettler, and Trigubovich 2010)

$$h_t = \sqrt{2t\rho/\mu}\,. \tag{1}$$

For example, at the resistivity of ρ = 100 Ω·m, $\mu = 4\pi 10^{-7}$ H/m, and t = 1 ms, the depth h_t ~400 m; at ρ = 1 Ω·m, h_t ~40 m. h_t does not depend on the antenna size $L\times L$; however, L forms the amplitude E_r of the measured response ($E_r \sim L^4$). Therefore, for small antennas registration of the transient response for long times is problematic due to the unfavourable signal/noise ratio. As a rule of thumb, the maximum depth is h_{max} ~3 L.

Once the transient response of $E_r(t)$ is measured, it can be transformed in the dependence of apparent resistivity $\rho\alpha(t)$ from the time by the formula (Barsukov *et al*. 2007) :

$$\rho_a(t) = \left[\frac{\mu^{3/2}L^4}{20\pi^{3/2}}\frac{I}{t^{5/2}E_r(t)}\right]^{2/3} \tag{2}$$

Here, I is the amplitude of the pulse of electric current, and L is the side of the square antenna. Formula (2) adequately describes the resistivity of the medium at later times but distorts this value at early times. As such, the responses can be analysed and compared with data from other methods of electrical soundings, such as VES.

Examples of transient responses in the form of an apparent resistivity for three points of soundings: Sp-24, Sp-40, and Sphinx are shown in Fig. 2 (lower panel). In the TEM-FAST technology, the transformation of the responses to the apparent resistivity versus depth $\rho(h)$ is applied. The algorithm of the transformation comprises three successive stages:

(i) Approximation of the $E_r(t)$ responses with an $E(t)$ function, which is the sum of the exponential functions decreasing in time (Svetov and Barsukov 1984):

$$E(t) \approx E_r(t) = A_1 e^{-t/\tau_1} + \ldots + A_N e^{-t/\tau_N} \tag{3}$$

The A_i and τ_i (i=1,..., N) parameters minimize a discrepancy between $E(t)$ and $E_r(t)$. Thus, the experimental data are approximated by the analytical and infinitely differentiable function $E(t)$.

(ii) Calculation of resistivity ρ of the uniform half-space, the response of which coincides with $E(t)$ at each time t:

$$E(t) = M\{\rho(t)\} \tag{4}$$

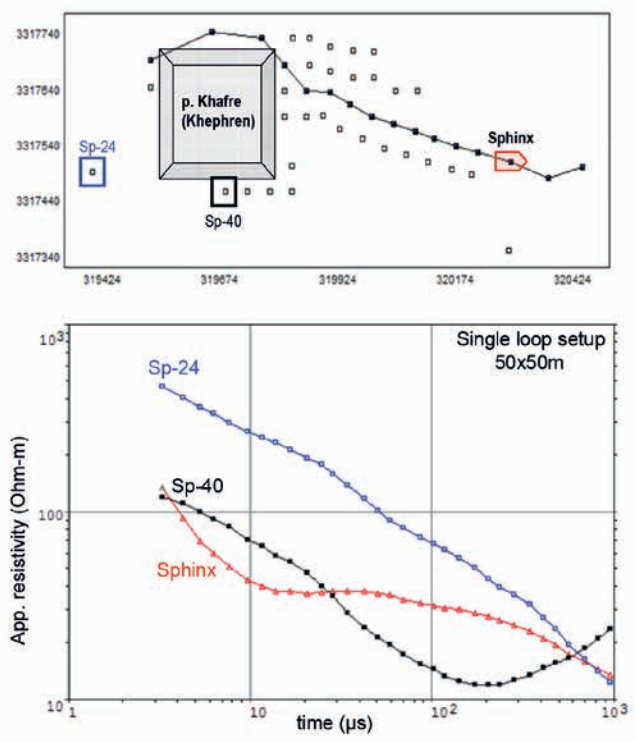

Figure 2 Location of TEM points in the study area (upper panel) and the transient responses in the form of apparent resistivity (lower panel). The broken line denotes the profile analyzed in Fig. 4.

$M\{\ \}$ is an operator that computes the EM response of uniform half-space that has a resistivity $\rho(t)$ at a time t (t is defined as a fixed parameter). The formula to rapidly calculate the transient response $M\{\rho\}$ for a combined antenna was given in (Barsukov *et al*. 2007). The one-dimensional nonlinear equation (4) with respect to ρ for each time t was solved via the quickest descent method. The dependence $\rho(t)$ adequately reflects the true environmental resistance as in later and earlier times.

If the medium is uniform, then $\rho(t)$ does not change with time and coincides with its resistivity. Figure 3(a) presents the responses $\rho_a(t)$ and $\rho(t)$ computed at the second step of the transformation.

(iii) Calculation of the parametrically specified function $\rho(h)$ for each parameter t; the logarithmic derivative ν and coefficient $k(t)$ are computed first:

$$\nu = \frac{t}{\rho\ (t)}\frac{d\rho(t)}{dt} = \frac{d\ln\rho(t)}{d\ln t}\ ,\quad k(t) = \frac{1}{(1\text{-}\nu)^{3/2}}\qquad |\nu| < 1. \tag{5}$$

Then, the apparent resistivity $\rho(h)$ and depth h of the investigation are computed:

$$\rho(h) = k(t)\rho(t)\,,\qquad h = \sqrt{t\frac{k(t)\rho(t)}{\mu}}\,. \tag{6}$$

Figure 3(b) demonstrates an example of $\rho(h)$ transformation. The transformations smooth the piecewise uniform distribution of the

resistivity ρ and depth h, at that they slightly distort ρ and h. Nevertheless, the basic features of the model are preserved. In addition, it is important that the design of a stable transformation requires no *a priori* information about the medium. Local 1D transformations $\rho(h)$ that are "stitched" in 2D or 3D structures create an image of the EM medium; in the 2D case, the image is called a "pseudo-section."

The next step in building the 3D model is the projection of the transformations onto a vertical grid of the model that is replacement of the continuous function $\rho(h)$ (Fig. 3) with a stepped piecewise approximation. Several tens of layers with different resistivities may be necessary, depending on the details of the required research. The grid of the 3D model analysed here consisted of uniform cells of $\Delta x = \Delta y = 25$ m and $\Delta z = 2$ m.

The finite difference discretization scheme for a 3D model is described in AEMR (2014) and illustrated in the Appendix. Figure 4(a) shows a section of the 3D model that is "stitched" from the 1D local models. The resistivities between the observation points are linearly interpolated in horizontal directions on a more dense square grid Dx=Dy. The profile position is shown in the upper panel of Fig. 2. The upper panel of Fig. 4A shows the experimental data and the calculated responses of the 3D model. The discrepancy between the observed and modelled data decreased, but it still leaves much to be enhanced.

At the next step, the 1D inversion of the responses is fulfilled in a class of multilayer local models. Details of this process are set out in the Appendix. In the process of the 1D inversion, the resistivities of the layered structures are fitted to minimize the discrepancy between the observed and calculated responses at each measuring point. The modified Levenberg–Marquardt algorithm (e.g., Pujol 2007; Barsukov *et al.* 2007) have been used for the inversion. The result of the inversion along the profile is shown in Fig. 4(b). The upper panel shows the experimental data and the calculated 3D responses. The discrepancy between the observed and modelled data decreased, but it still leaves much to be desired.

At the next stage of the inversion, the model was separated into several homogeneous blocks. The code TEM-3D-WIZARD (AEMR 2014) uses the finite-difference time-domain algorithm proposed by Druskin and Knizhnerman (1988, 1994), which allows us to determine the resistivities without changing the geometric boundaries for the 3D block model of the medium. Because the code works in parallel on multi-core PCs, the time to compute a response to an accuracy of ~3% is less than 1 s using an eight-core laptop with a 2.2-GHz processor.

After the final stage of the 3D inversion, the discrepancy between the observed and modelled responses is minimized, and the resistivities of the blocks are matched without changing their boundaries. In this case, the inversion is performed with respect to ten values of resistivity within 1 Ω·m–1000 Ω·m. The result is shown in Fig. 4(c). The misfit between the observed and modelled data was within 12% for $t = 250$ μs. The total residual (rms) throughout the whole time range was ~8%, which is generally

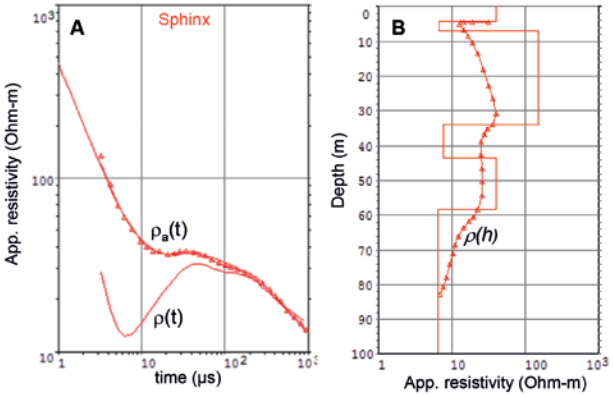

Figure 3 (a) Transient responses (triangles) in the form of apparent resistivity $\rho a(t)$ (formula 2) and $\rho(t)$ (formula 4). (b) Dependence of the apparent resistivity of the depth h of the investigation (formula (6)); the piecewise curve is the result of the 1D inversion of the response obtained when the sounding area beneath the Sphinx.

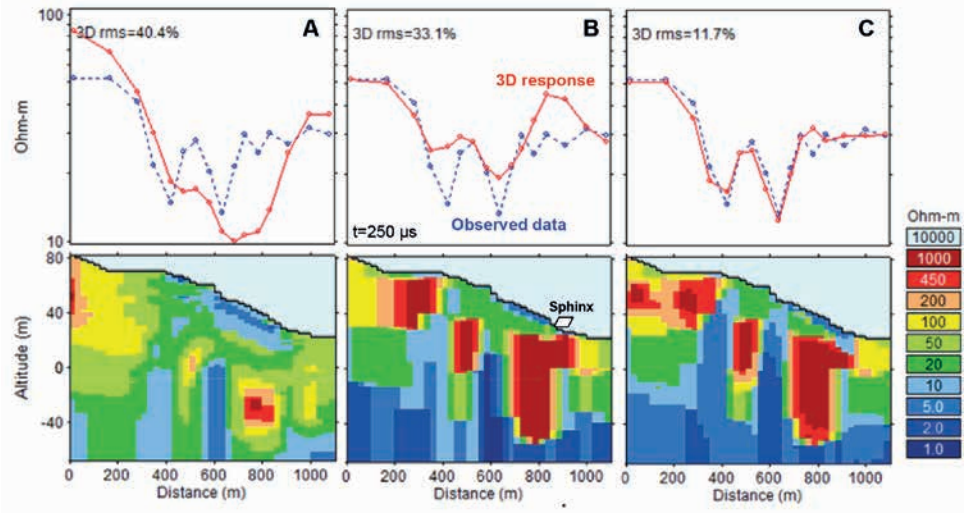

Figure 4 The sections of resistivity for the 3D model along the profile that is shown in Fig. 2. (a) Structure created on the basis of transformations $\rho(h)$. (b) The structure created on the basis of local 1D inversions. (C) Result of the 3D block inversion. The upper panels show the apparent resistivity to experimental and model responses for $t = 250$ μs.

commensurate with errors of the survey. From the analysis of the inversion results at various stages, one can see that the main feature of the model appears in the initial phase of the transformation (Fig. 4a): three blocks of high resistivity are broken by sub-vertical low-resistive ruptures. The sections shown in panels (b) and (c) are not fundamentally different, but their 3D responses are more contrasting and in better agreement with the observed data. Figure 5 shows horizontal sections (slices) of the final 3D resistivity model.

Analysis of the geoelectric model

The completed 3D model exhibits the following characteristics. The resistivity of the surface layer (first 5 m) ranges from 10 Ω·m to 500 Ω·m and reaches a minimum to the east of the Sphinx (Fig. 5a). This result is entirely consistent with the VES data obtained in the vicinity of the monument (± 100 m). Here, the resistivity does not exceed 20 Ω·m in range of AB/2 < 5 m. With an increasing depth of ~10 m below the surface, the resistivity of rocks rises, as confirmed by VES (NRIAG 1993).

On the horizon of 0 m mean sea level (MSL), the centre and south flank of the territory have a resistivity of more than 200 Ω·m, whereas the north flank has resistivity of ~10 Ω·m–20 Ω·m (Fig. 5b). In the central part, a low-resistive seam 30 m–50 m thick is traced in the SW–NE direction. On the horizon of ~50 m MSL, the resistivity falls to 5 Ω·m–10 Ω·m, except in two regions (Fig. 5c). At a deeper horizon of ~100 m MSL, a single block at the southern edge of the p. Khephren with a resistivity of more than 200 Ω·m is observed against the background of an almost uniform medium with a resistivity of less than 10 Ω·m.

On the vertical section of the model (Fig. 4c), three blocks of rocks with resistivities of more than 200 Ω·m that are separated by sub-vertical seams with a resistivity of less than 10 Ω·m are observed. All blocks are underlain by rocks with a resistivity of less than 10 Ω·m. To the east, the thickest block of the Sphinx is traced to the ~50 m MSL horizon.

GEOLOGICAL INTERPRETATION OF THE MODEL

The Giza Pyramid plateau is composed of Middle Eocene limestone of the Mokattam formation; in the region, rocks of this horizon only occur at the plateau (Said 1962). Limestones monoclinally fall in the SE direction at an angle of 5°–7°. The Mokattam stratum are inconsistently underlain by carbonates from the late Cretaceous, which were intensively crushed as a result of late Cretaceous tectonic activity. Raynaud *et al.* (2010) demonstrated fragments of a geological map, which showed a complex folded structure called Abu Rowash (9 km NW of the Pyramid plateau) composed of Cretaceous rocks that exclude the Mokattam formation. The Cretaceous sediments are covered with the younger rocks of the Upper Eocene Maadi formation. The thickness of the Mokattam formation is not defined. In the NW direction, the Mokattam base is exposed on the +100 MSL horizon 2.5 km from the Pyramid plateau. If we assume that the base of the column is flat, then it is possible to estimate the maximum thickness of the Mokattam formation under the Sphinx (+25 m MSL): Hmax ~190 m–280 m at the angles of the dip of 5°–7° SE.

As shown in Fig. 5, the resistivity of rocks in the created 3D model changes by almost three orders and contradicts the assumption that only a laterally uniform layer of limestone is present. Such sharp vertical heterogeneity of the resistivity can be explained by the complex topography of the underlying strata of the Cretaceous sediments. For example, in the structure of Abu Rowash, the rock units change the angle and dip vector from 15° SE to 15° NW at a distance of approximately 2 km to form a "mini depression" with a ~250 m depth. This folded structure also underlies the Pyramid plateau (Gauri 1984; Raynaud *et al*. 2010).

Thus, the resistive blocks of the model are composed of dense limestones of the Mokattam formation and are broken by a flooded fault area in the SW–NE direction. The maximum thickness of the dense limestones under the southern edge of p. Khephren (+65 m MSL) is at least 160 m (Fig. 5d); near the Sphinx (+25 m MSL), the maximum thickness is approximately 80 m. The low-resistive underlying horizons are crumpled in folds of fractured carbonates of the Cretaceous and are saturated with saline water.

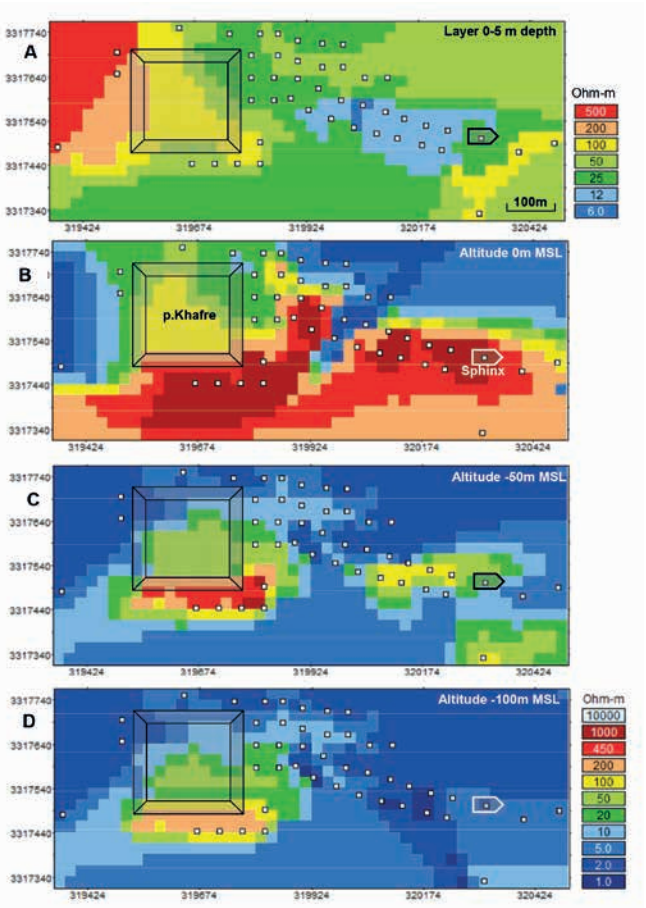

Figure 5 The horizontal sections of the 3D resistivity models for different altitudes (MSL). The average resistivity of the surface layer with a thickness of (a) 5 m, (b) 0 m, (c) 50 m, and (d) 100 m.

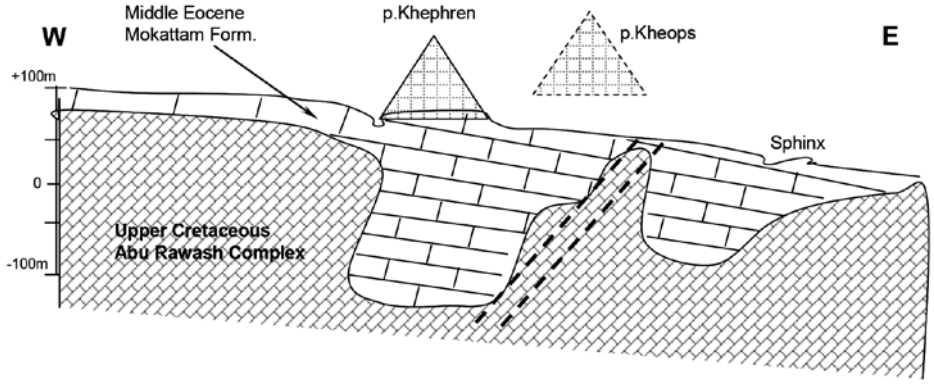

Figure 4 The sections of resistivity for the 3D model along the profile that is shown in Fig. 2. (a) Structure created on the basis of transformations $\rho(h)$. (b) The structure created on the basis of local 1D inversions. (C) Result of the 3D block inversion. The upper panels show the apparent resistivity to experimental and model responses for $t = 250$ μs.

In the western part of the plateau (0.5 km–1 km to the west of p. Khephren), where the "calibration" soundings were made, the transient responses are similar to the Sp24 (Fig. 2), i.e., the resistivity ρ of the surface layer (25 m) is greater than 500 Ω·m; a further 100-fold drop of the resistivity to 5 Ω·m at a depth of 45 m and up to 1 Ω·m at a depth of 70 m occurs. It is clear that the top layer corresponds to dense low-permeability limestone and that the underlying strata presents fractured rocks saturated by mineralized water. Thus, the boundary of the high- and low-resistive formations created in the model corresponds to the boundary of the Cretaceous and Paleogene sediments. A schematic geological cross section of the pyramid's plateau along the line from the Sphinx to p. Khephren is shown in Fig. 6.

Note that the results of the "calibration" measurements and the responses recorded on the main territory of the study indicate the absence of significant errors in the electromagnetic (EM) survey caused by the numerous man-made objects on the plateau pyramids.

As shown in Fig. 5(a), the 5-m-thick surface layer of the Mokattam limestone is characterized by a very heterogeneous electric resistivity. The area to the west of the Sphinx has a resistivity of approximately 12 Ω·m, which corresponds to the VES data (NRIAG 1993). Gauri (1984) and Guirand and Bosworth (1999) noted that the lower unit of the Mokattam formation (the base of the Sphinx) presents Argillaceous limestone with evaporite minerals, such as halite, whereas the upper unit (p. Khephren) features massive reefal (bioherm) limestone. In our opinion, the reduced resistivity of the surface layer is due to the high clay content and the salinity of carbonates.

CONCLUSIONS

A 3D geoelectric model based on transient electromagnetic method (TEM) soundings was created for the plateau of the Great Pyramids, located within the area from p. Khephren - p. Cheops and the Sphinx. The 3D block inversion technology was used to design this model. This technology consists of successive applications of transformation of transient responses and local 1D inversions, which reconnoitre the major rock block boundaries in the modelled medium and, during the final stage, determine the electrical resistivity of the selected blocks. The ability for such an approach to interpret the TEM data was demonstrated using a 3D calibration model of the structure medium near the plateau of the Pyramids. The created plateau model indicated the thickness of the slightly inclined Mokattam limestones varied from 25 to 150 m within a 1000 × 300 m^2 area. Such intense changes in the limestone subface's altitudes were controlled by the folded structure of the underlying Cretaceous carbonates. Cretaceous carbonates show low electrical resistivity, which is typical for fractured rocks saturated with saline water. Dense Mokattam limestone blocks are broken by water-saturated zones with sub-vertical faults in the SW–NE direction. The electrical resistivity in the carbonate surface layer, which lies at the base of the pyramids and the Sphinx, is heterogeneous with a composition that depends on the clay content and presence of halite.

ACKNOWLEDGEMENTS

The authors would like to thank NRIAG and Prof. B.S. Svetov, for their help with the field work; the company AEMR Ltd. (the Netherlands), for the opportunity to use the computer code for the 3D data inversion of the TEM soundings; and the reviewers for helpful comments and suggestions.

REFERENCES

AEMR. 2014. *TEM-3D-WIZARD, 3D Manual*, pp 50. www.aemr.net.

Barsukov P.O., Fainberg E.B. and Khabensky E.O. 2007. Shallow investigation by TEM-FAST technique: methodology and case histories. In: *Methods of Geochemistry and Geophysics*, *Vol. 40* (ed. V.V. Spichak), pp. 55–77. Elsevier.

Barsukov P.O., Hassaneen A.Gh., Svetov B.S. and Osman S.Sh. 1996. Geoelectrical Study in the vicinity of Giza Pyramids, Egypt. In: *13th Workshop on Electromagnetic Induction in the Earth*, Japan.

Druskin V. and Knizhnerman L. 1988. A spectral semi-discrete method for the numerical solution of 3D non-stationary electrical prospecting problem. *Physics of the Solid Earth* **24**, 641–648.

Druskin V. and Knizhnerman L. 1994. Spectral approach to solving three-dimensional Maxwell's equations in the time and frequency domains. *Radio Science* **29**(4), 937–953.

Kamenetsky F.M., Stettler E.H. and Trigubovich G.M. 2010. *Transient Geo-Electromagnetics*, pp. 304. EAGE, Munich, Germany.

Gauri K.L. 1984. Geologic study of the Sphinx. *ARCE Newsletter* **127**, 24–43.

Guirand R. and Bosworth W. 1999. Phanerozoic geodynamic evolution of northeastern Africa and the northwest Arabian Platform. *Tectonophysics* **315**(1–4), 73–108.

National Research Institute of Astronomy and Geophysics. 1993. *Report of the First Six Months of Underground Water Monitoring at Sphinx Area to Egyptian Authority of Monuments, June 1993, Egypt.* NRIAG.
Pujol J. 2007. The solution of nonlinear inverse problems and the Levenberg-Marquardt method. *Geophysics* **72**(4), W1–W16.
Raynaud S., Boisse H., Makroum F.M. and Bertho J. 2010. Geological and Geomorphological study of the original hill at the base of Fourth Dynasty Egyptian monuments. *Bulletin de la Societe Geologique de France* **181**(3), 279–290.
Said R. 1962. *The Geology of Egypt,* pp. 377. Elsevier, Amsterdam–New York.
Svetov B.S. and Barsukov P.O. 1984. Transformation of the quasi-stationary transient processes in the geoelectrically equivalent waves. *Physics of the Earth* **8**, 29–37.
Zhdanov M.S. 2009. *Geophysical Electromagnetic Theory and Methods.* Elsevier, pp. 680.

Appendix A. The block 3D inversion technology

In this section, we describe the block 3D inversion process for transient electromagnetic (TEM) data in detail and determine how well the resultant geoelectric model corresponds to the "true" model. For this purpose, we constructed a simple 3D calibration "true" model. Two 2D sections in the model are shown in Fig. A-1. The model has a 2D syncline in its centre with a 3D peak at a depth of 130 m with a 300 × 300 m^2 square base section and X × Y = 100 × 300 m^2 rectangular section at the top (depth = 40 m).

Figure A-2 shows the 2D section along the profile (Y = 0) crossing the centre of the model and the grid used for the calculations. The TEM-3D-WIZARD program was used to calculate the transient responses for a 50 × 50 m coincident antenna using 7×61 points along seven profiles, where X = (–1500 m, +1500 m) and Y = (–300 m +300 m), within the time range from 1 μs–1000 μs. The calculation accuracy did not exceed 3%. The profile step size along the X axis equalled the antenna size, i.e., 50 m, the distance between the profiles (along the Y axis) was 100 m. The calculated "experimental" responses were transformed to $\rho(h)$ and projected onto the model grid. Adjacent thin layers with contrasting longitudinal conductivities, $S = h/\rho$ (thickness divided by resistivity), below 10% were combined into thicker layers.

Two sections in the resultant "stitched" projections, $\rho(x, y, z)$, are shown in Fig. A-3. The distribution for $\rho(x, y, z)$ was used as the starting model for the point-wise local 1D inversions. The layer thicknesses in the 1D models were fixed. The 1D inversion results were stitched into a single 3D structure, as shown in Fig. A-4.

Figure A-4 indicates the majority of blocks in this model (10 Ω·m < ρ < 95 Ω·m) had no significant longitudinal conductivity S and transitioned from a high to low resistivity. This resistivity distribution with fixed block boundary geometries was used as the start for the 3D inversion. During the inversion process, the code calculated the transient responses at each of 7×61 observation points to minimize the discrepancy between the original and model data. The calculated misfit between the "experimental"

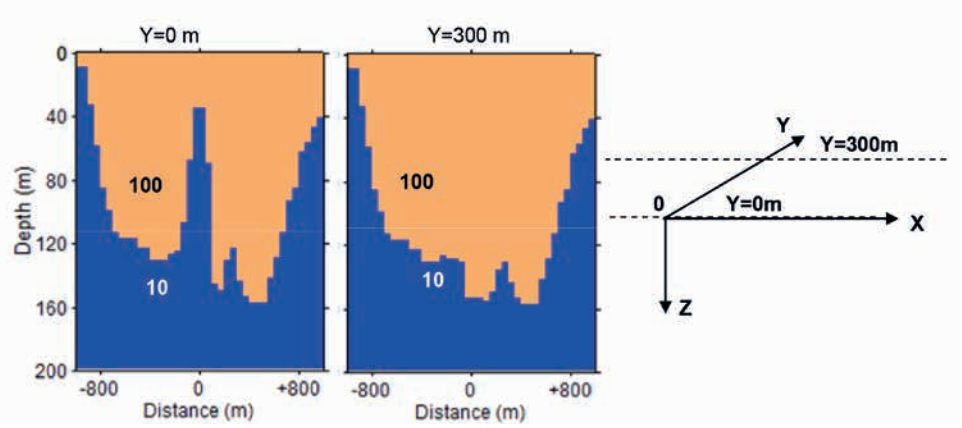

Figure A-1 The 2D sections from the 3D model along the X-axis. The Y=0 profile passes over the centre of the model. The labels are the resistivities (Ω·m). The model was constructed using a grid with a step of Δx=Δy=25 m and Δz=2 m.

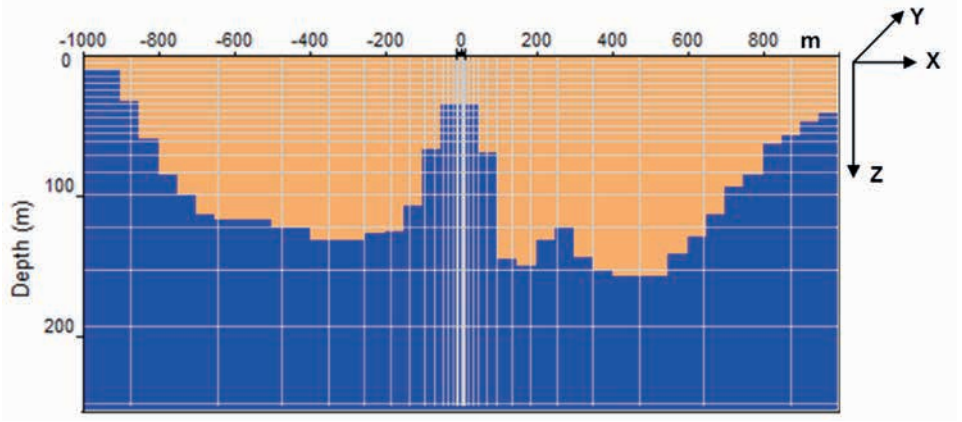

Figure A-2 The central profile for the model with varying grid spacing. There were X×Y×Z = 37×37×29 = 39701 cells.

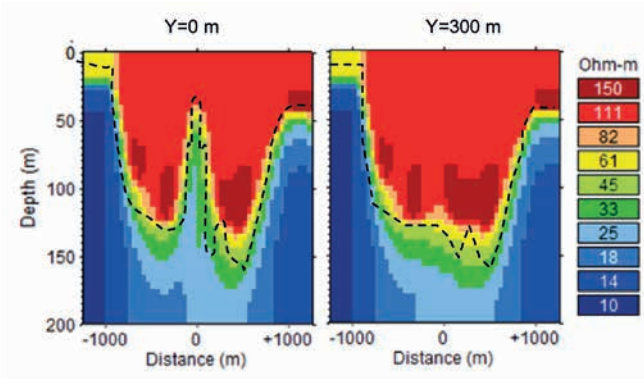

Figure A-3 Calculated $\rho(x, y, z)$ sections for the 3D model along two profiles at Y=0 m and Y=300 m; the dotted line is the calibration model boundary.

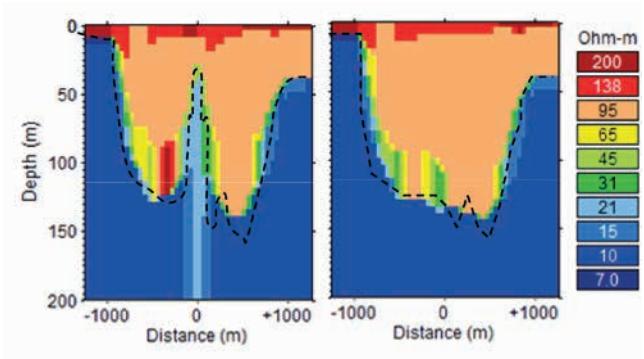

Figure A-4 Pointwise 1D inversion along two 3D model profiles. The black dotted line shows the calibration model boundary.

and modelled data was $\Omega = \| W(\rho_{\exp} - \rho_{\mathrm{mod}}) \|_{L_2}$, where $\rho_{exp} = \rho_{exp}(x, y, t)$ and $\rho_{mod} = \rho_{mod}(x, y, t)$ are the experimental and modelled transient responses using the apparent resistivity, $\| \|$ is the norm in L_2 space, and $W=W(x, y, t)$ is a weight function determined by the experimental uncertainty. The inversion process in this example was used to find the resistivity for the ten

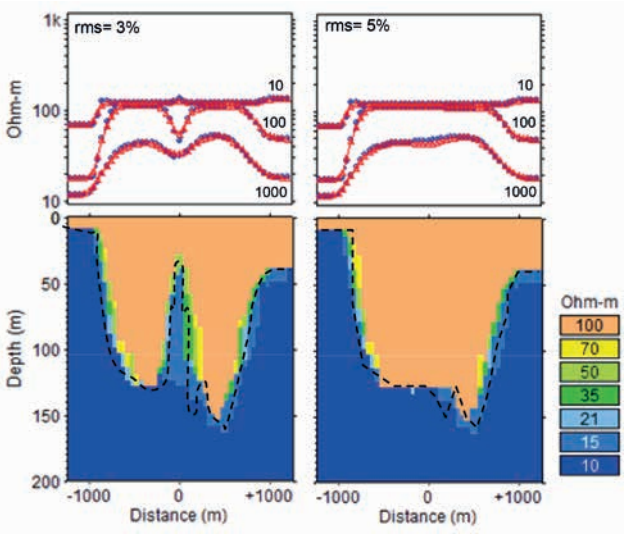

Figure A-5 Final 3D inversion along two profiles in the 3D model and the "experimental" and model apparent resistivity response at times t = 10, 100, and 1000 μs. The dotted line is the calibration model boundary.

blocks shown in Fig. A-4. The iterative process was stopped when the minimum W was achieved.

Figure A-5 shows the final inversion results (seven of the initial ten blocks remaining) and the experimental and modelled apparent resistivities for the three transient times along the Y=0 m and Y=300 m profiles. The mean misfit varied across the range from 3%–5% (rms) for all times and profiles, and approximately corresponded to the experimental uncertainty.

As one can see, despite the misfit between the experimental and modelled data being less than the uncertainty for the initial data, the results (A-5) are different from the original test model for the medium. However, these differences do not affect the overall image of the model from a geological viewpoint. Such tests are useful after inverting and interpreting experimental data to evaluate the possible uncertainty for the final result.